Results from the MIGDAL OTPC

Tim Marley

Imperial College London / Rutherford Appleton Laboratory

On behalf of the MIGDAL collaboration

RD51 WG2 – 19/06/2023

Outline

- Recap of the experiment
- Working with glass GEMs
- New camera readout
- Detector performance during multi-day long run.
- Preparations for neutrons

The Migdal effect

- Direct DM experiments exploit the Migdal effect to search for nuclear recoils below threshold.
- This rare atomic effect was predicted by A. Migdal in the 30’s/40’s and first observed in radioactive decays in the 70’s – but not yet recorded in nuclear scattering.
- We aim to achieve the unambiguous observation (and characterisation) of the Migdal effect using a low-pressure optical TPC.

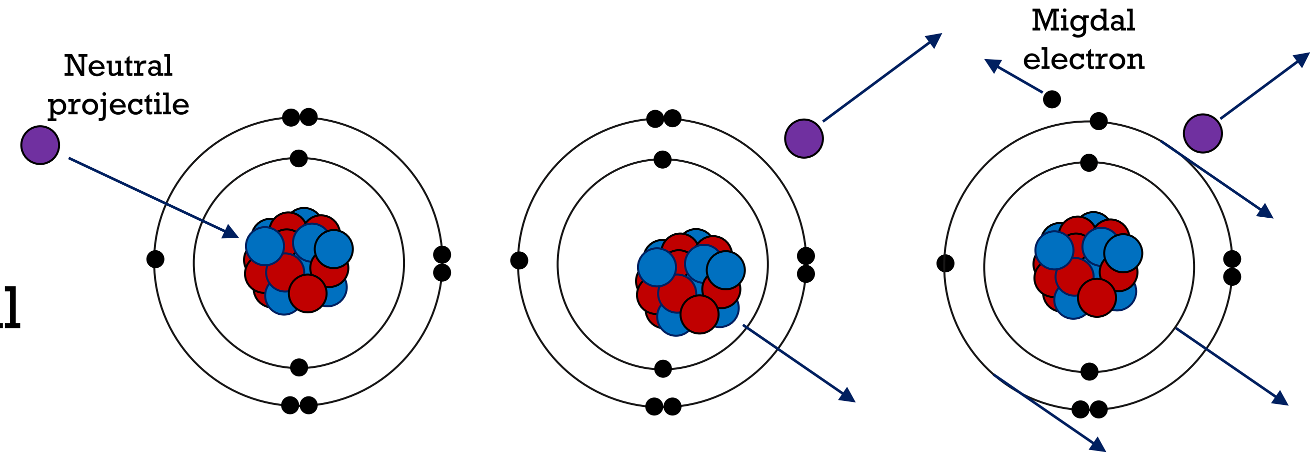

Migdal topology involves an electron and a nuclear recoil originating from the same vertex.

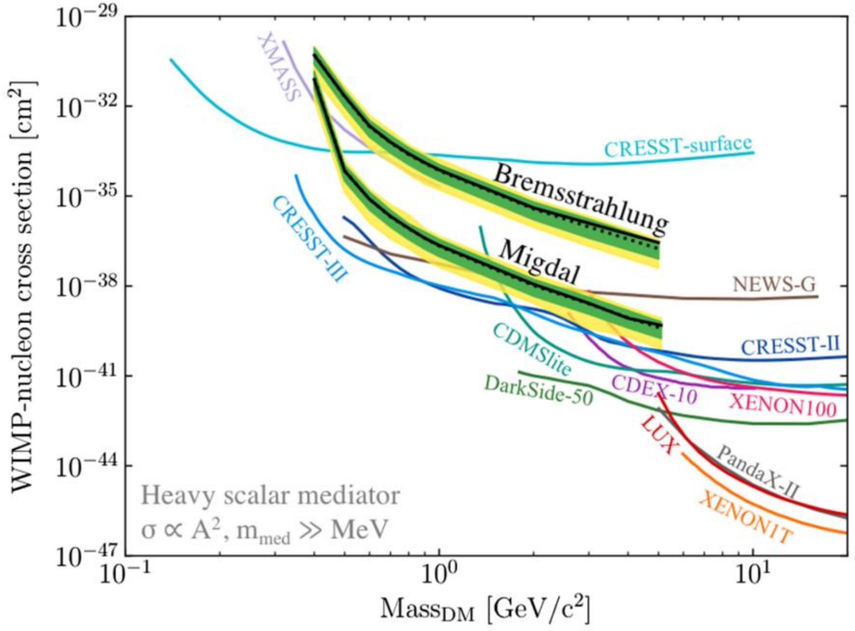

timothy.marley15@imperial.ac.uk

The MIGDAL experiment

- Low-pressure gas: 50 Torr of CF_4
    - Extended particle tracks
    - Avoid photon interactions
    - Can work with fraction of Ar
- Optical TPC
    - Amplification: 2x glass-GEMs
    - Optical: camera + photomultiplier tube
    - Charge: 120 ITO anode strips
- High-yield neutron generator
    - D-D: 2.47 MeV (10^9 n/s)
    - Defined beam, "clear" through TPC
- Electron and nuclear recoil tracks
    - Migdal: NR+ER tracks, common vertex
    - NR and ER have very different dE/dx
    - 5 keV electron threshold (Fe-55 calibration)

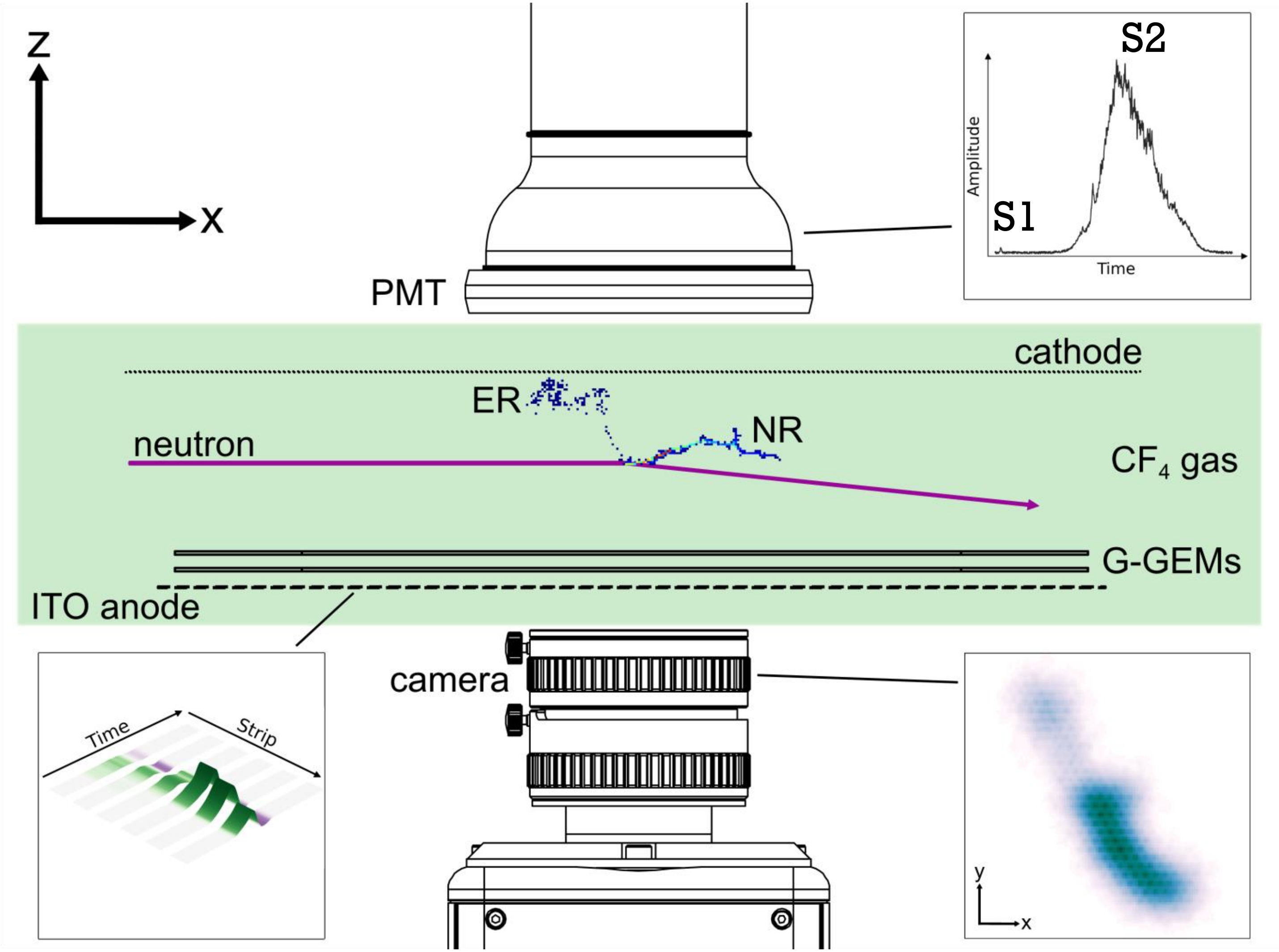

The MIGDAL optical-TPC

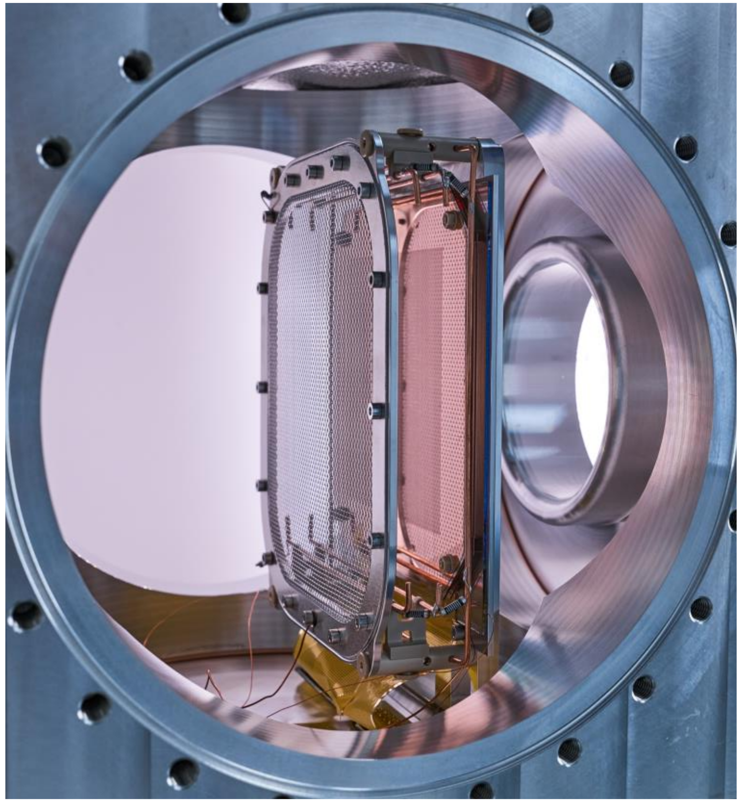

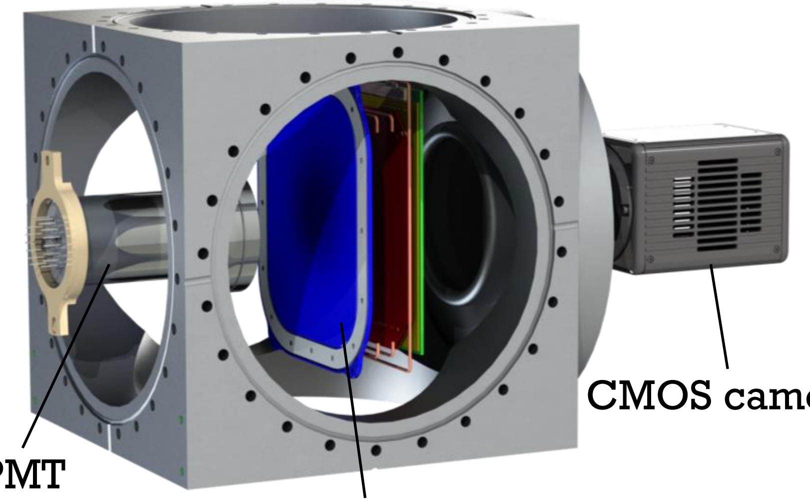

Cathode, GEM stack, ITO
$10 \times 10 \times 3\ cm^3$ active region
(compact!)

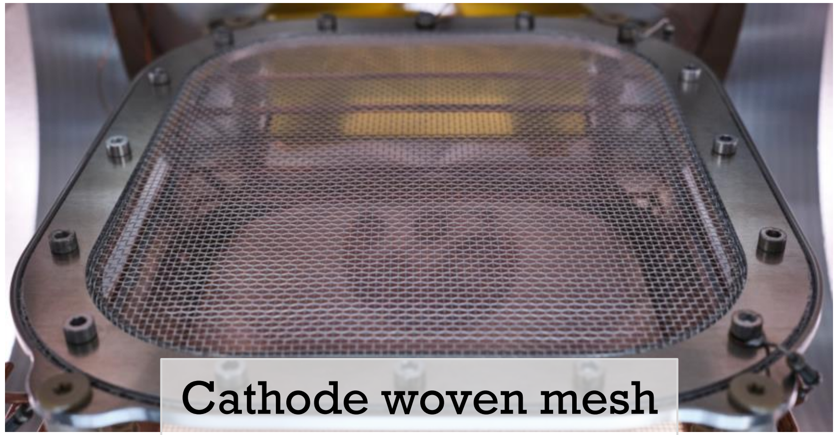

Cathode woven mesh
280 μm Al wire

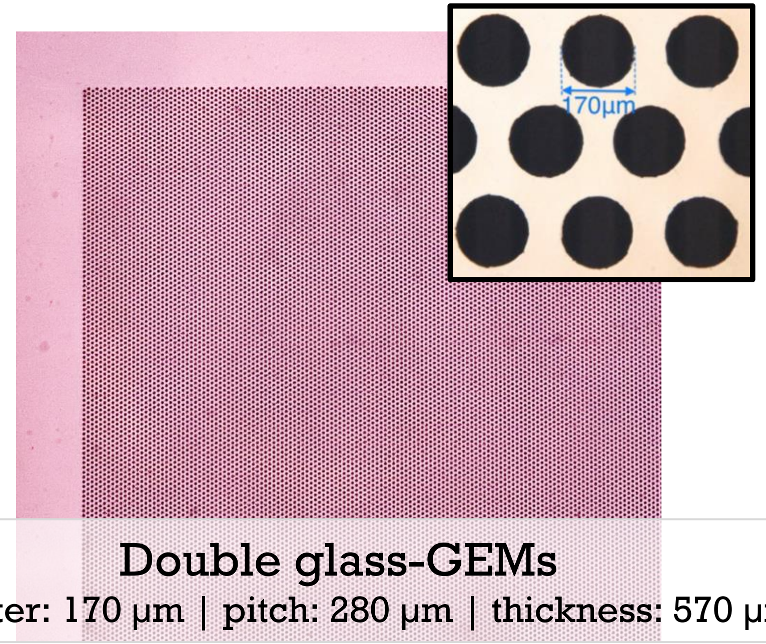

Double glass-GEMs
Diameter: 170 μm | pitch: 280 μm | thickness: 570 μm

Preparing G-GEMs

- We inspected for dust with a UV light and removed with a vacuum.
- We have G-GEMs with copper and nickel **(NEW!)** metallisation.
- In preliminary testing we noticed that at high voltages sparks were occurring on pillar support holes, not the active area.
    - The metallisation is quite jagged around these holes.

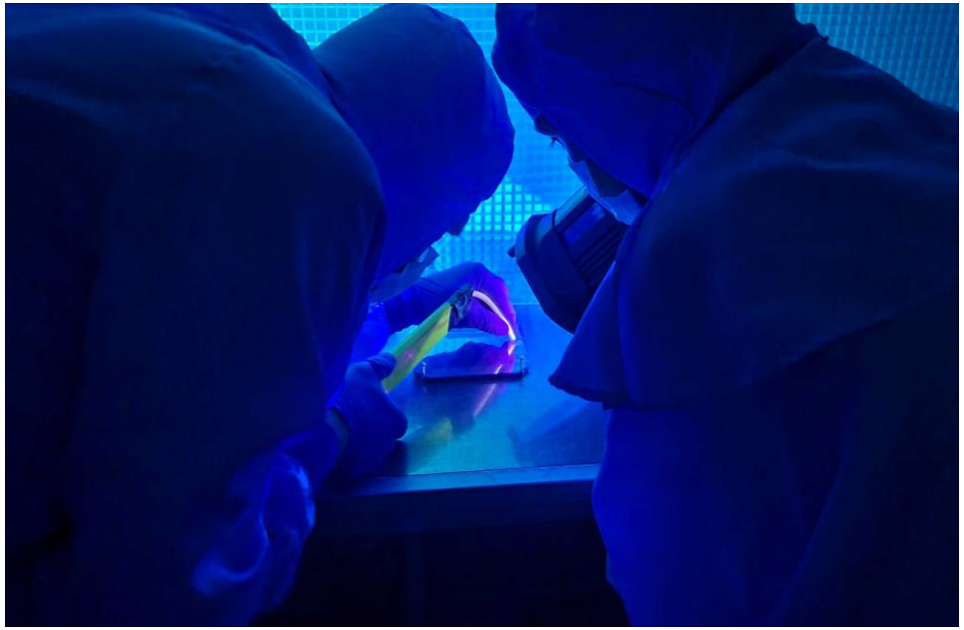

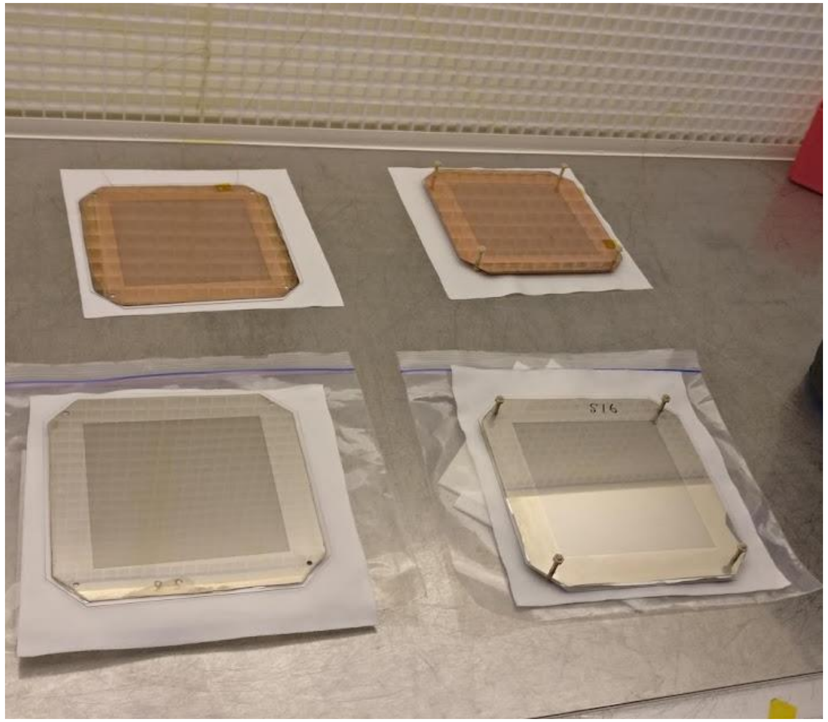

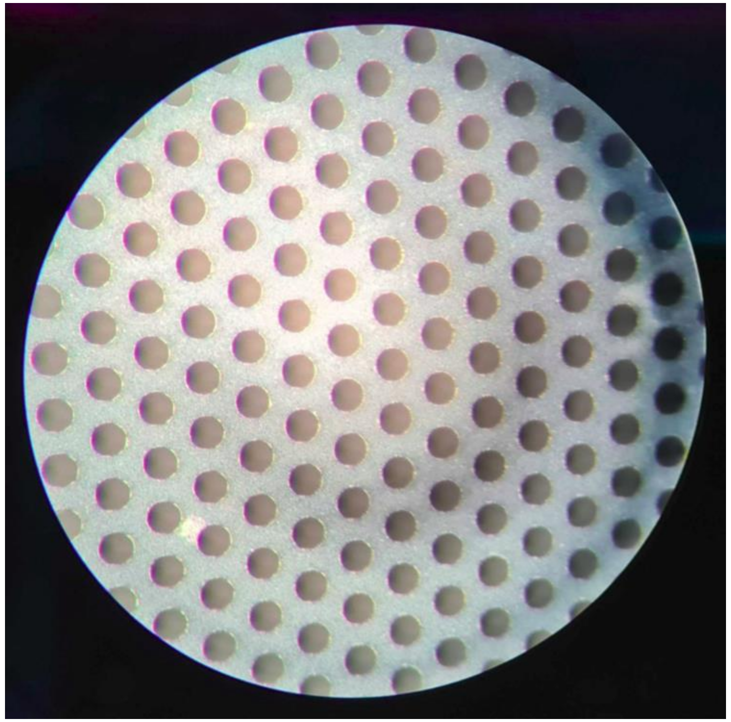

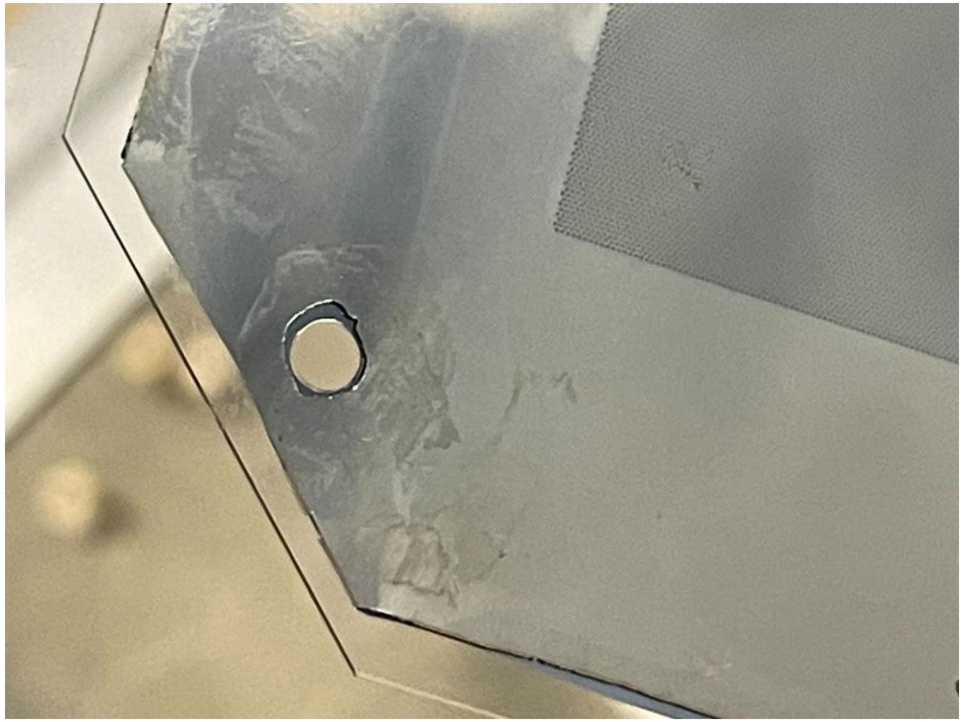

G-GEM resistivity

- We noticed the currents on our electrodes varying significantly with temperature.
- Checking an isolated G-GEM in a dry box showed the same effect.
- Our high-value protection resistors were causing problems as changes in G-GEM resistivity corresponded to significant changes in potential difference (~5 V).
- We altered the circuit and reduced the values of the protection resistors.

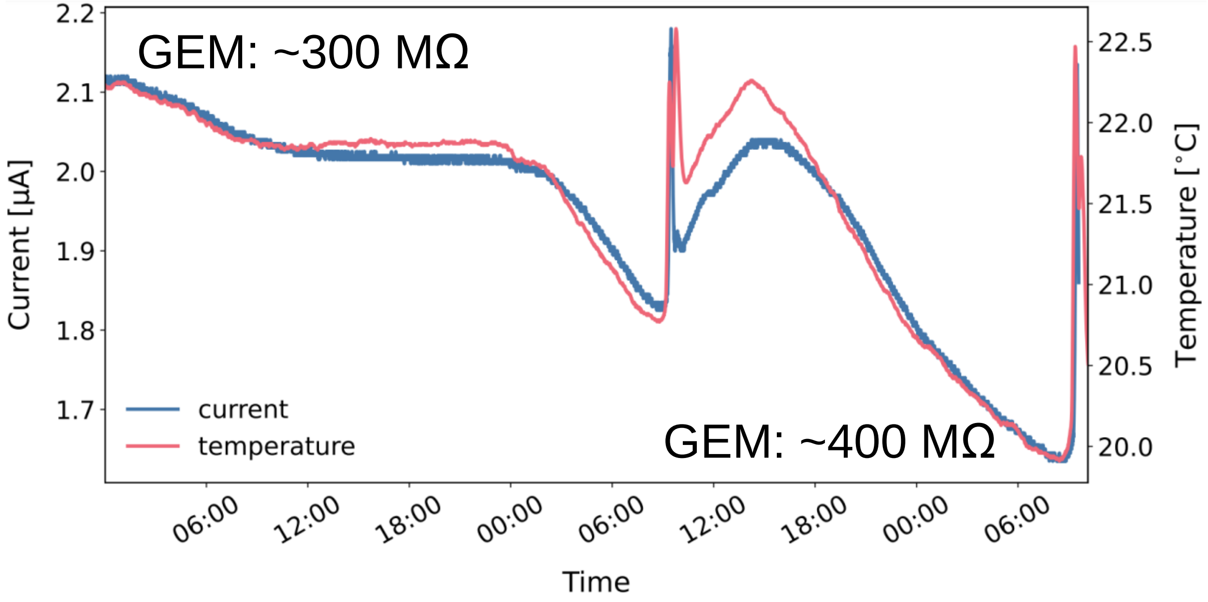

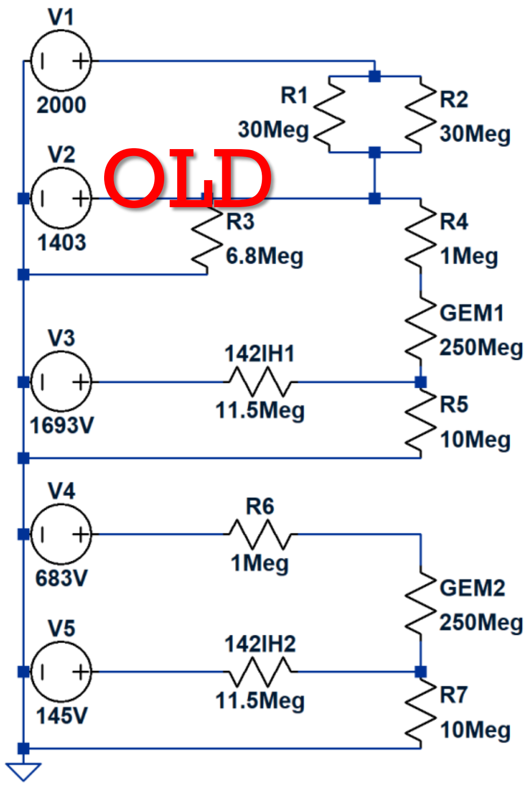

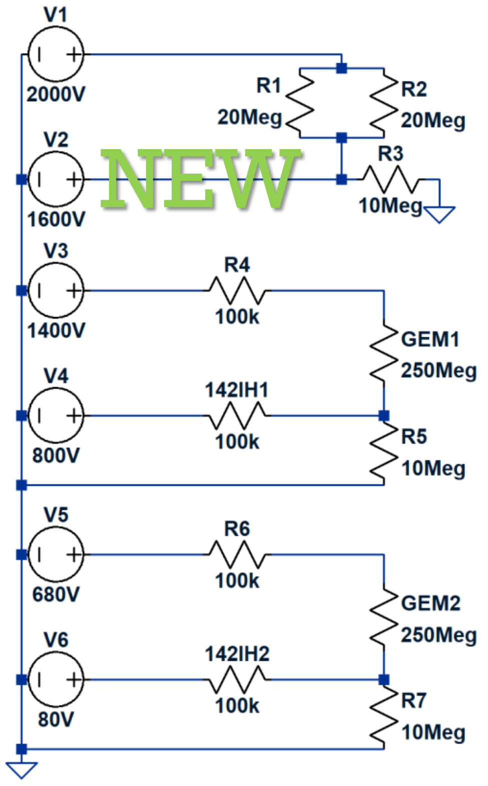

timothy.marley15@imperial.ac.uk

Detector readout

Charge readout

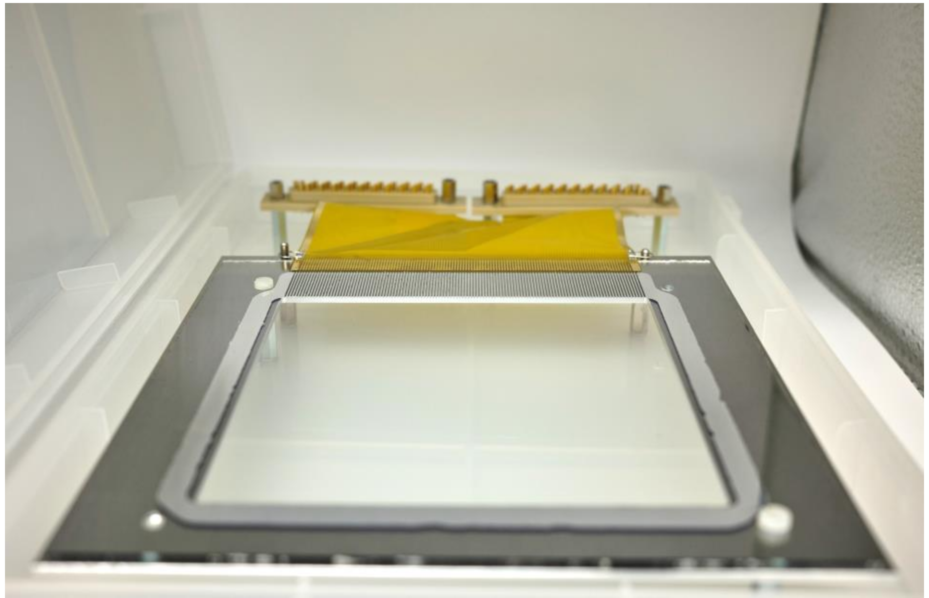

ITO anode strips
Post-GEM ionisation
Readout of (x,z) plane
Pitch: 833 μm
Digitised at 2 ns/sample
(Drift velocity: 130 μm/ns*)*

Optical readout

New camera!

qCMOS camera
(Hamamatsu ORCA - QUEST)
Detects GEM scintillation through glass viewport behind ITO anode
Readout of (x,y) plane
Exposure: 8.33 ms/frame (continuous)
Px scale: 39 μm (2×2 binning)
Lens: EHD-25085-C; 25mm f/0.85

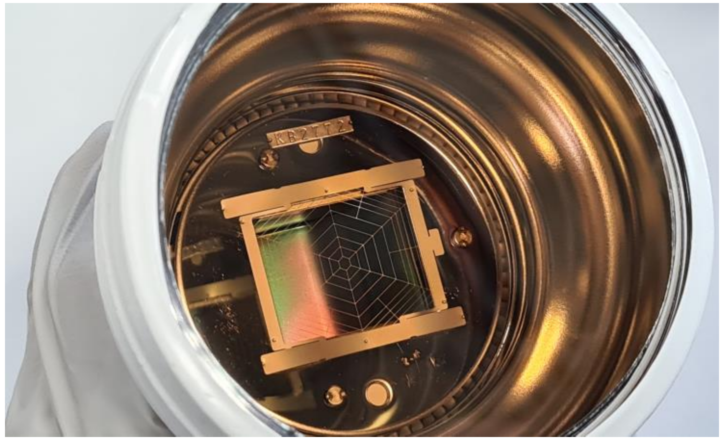

VUV PMT (Hamamatsu R11410)
Detects primary and secondary (GEM) scintillation
Absolute depth (z) coordinate
Digitised at 2 ns/sample
[Trigger]

timothy.marley15@imperial.ac.uk

Simulated camera readout (conservative gain)

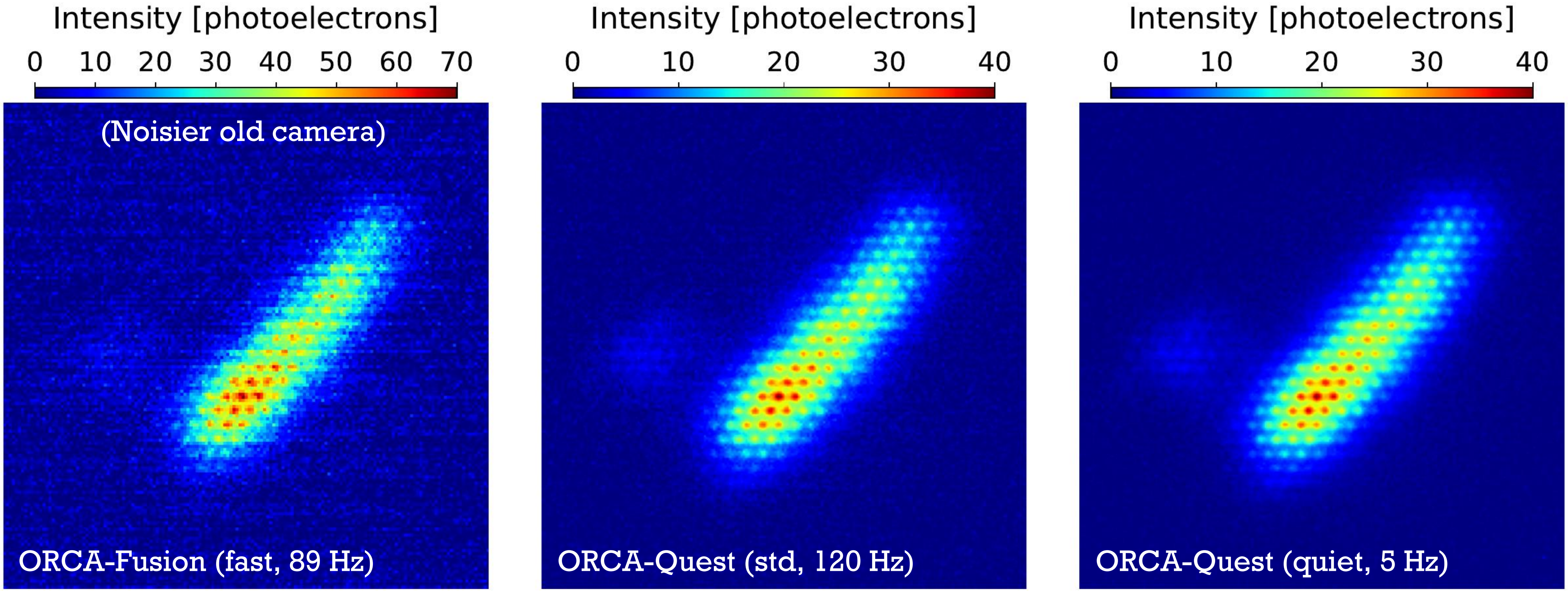

170 keV fluorine + 5.25 keV Migdal electron

Capabilities of the ORCA Quest

- The ORCA Quest is capable of ‘photon-number resolving’ at the cost of readout rate.
- We will not be using this mode for Migdal – risk of overlapping events.

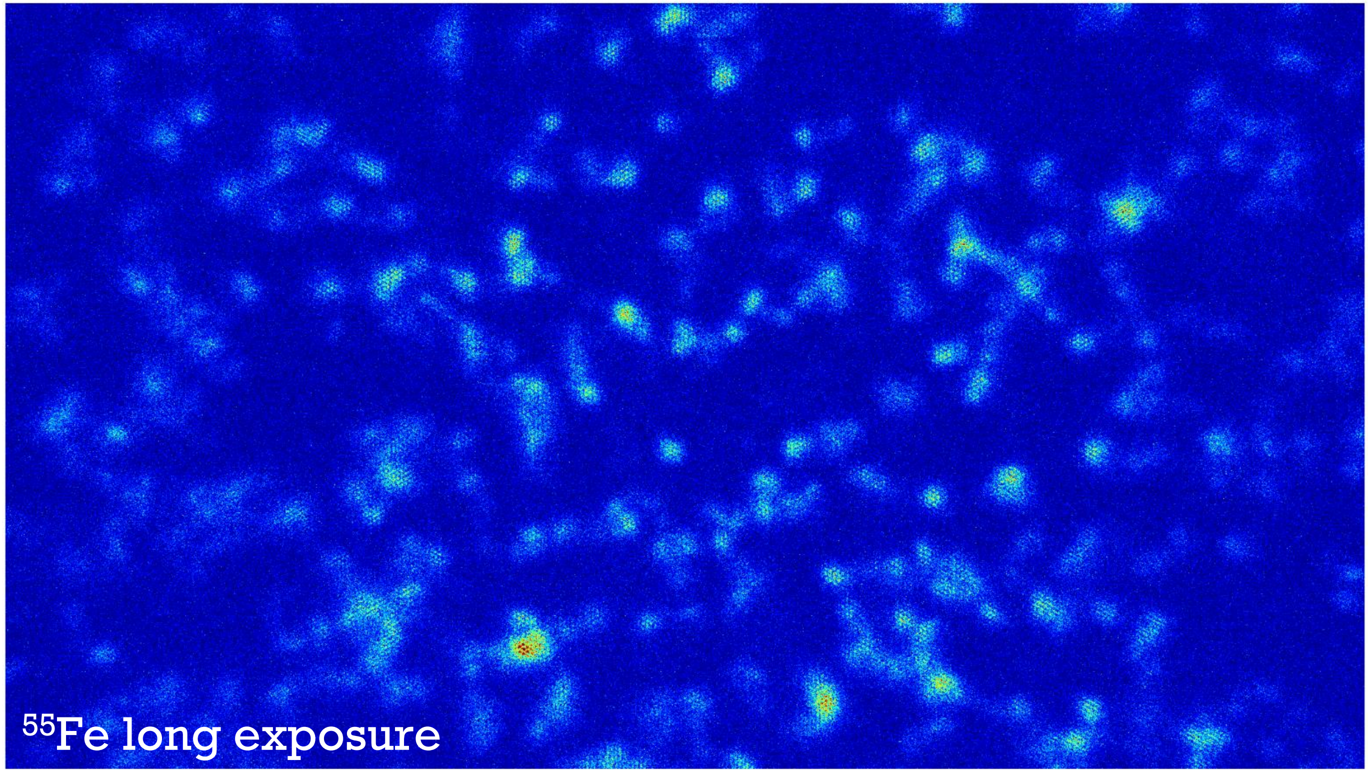

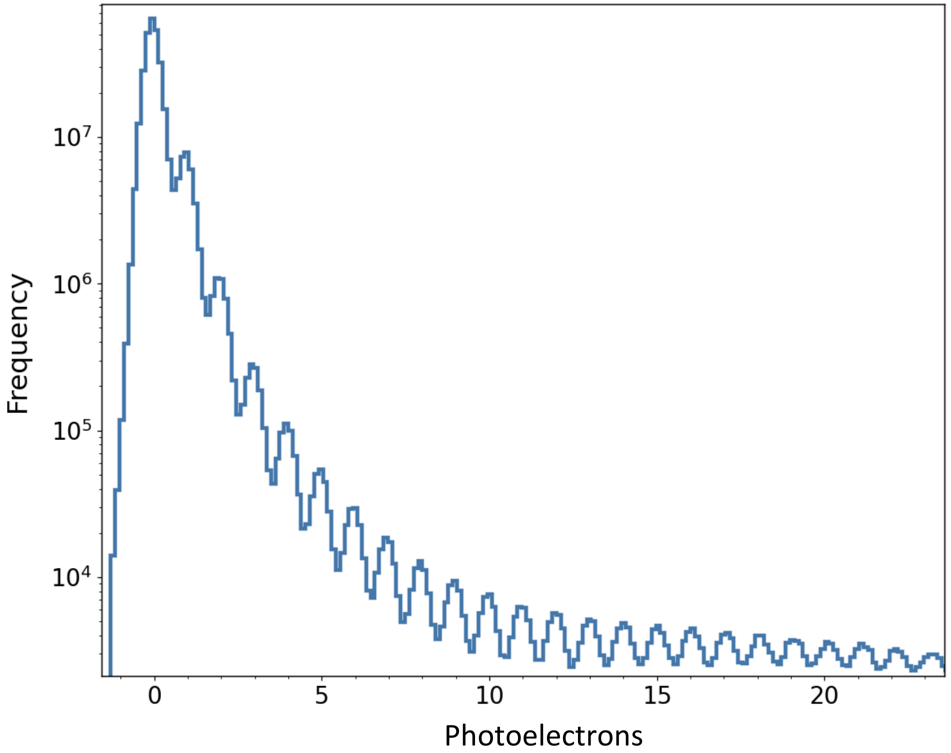

timothy.marley15@imperial.ac.uk

Comparison of the old/new cameras

- The noise is much more uniform and significantly lower on the Quest.
- Banding is more restricted to individual columns on the Quest.

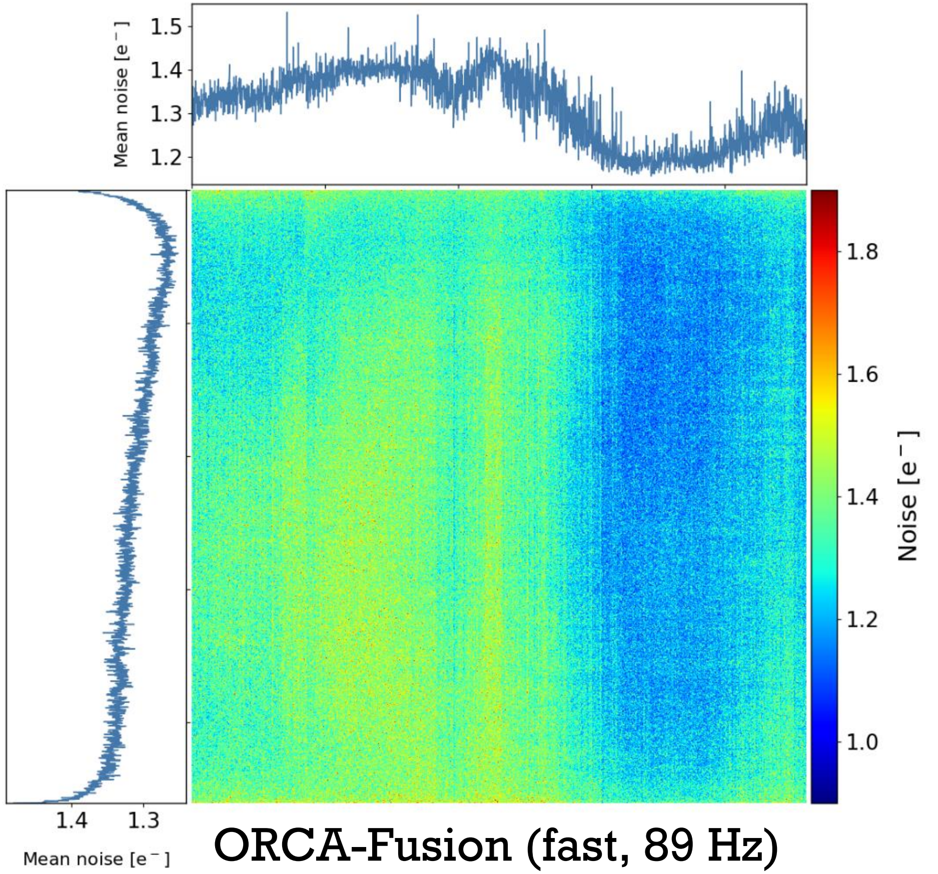

ORCA-Fusion (fast, 89 Hz)

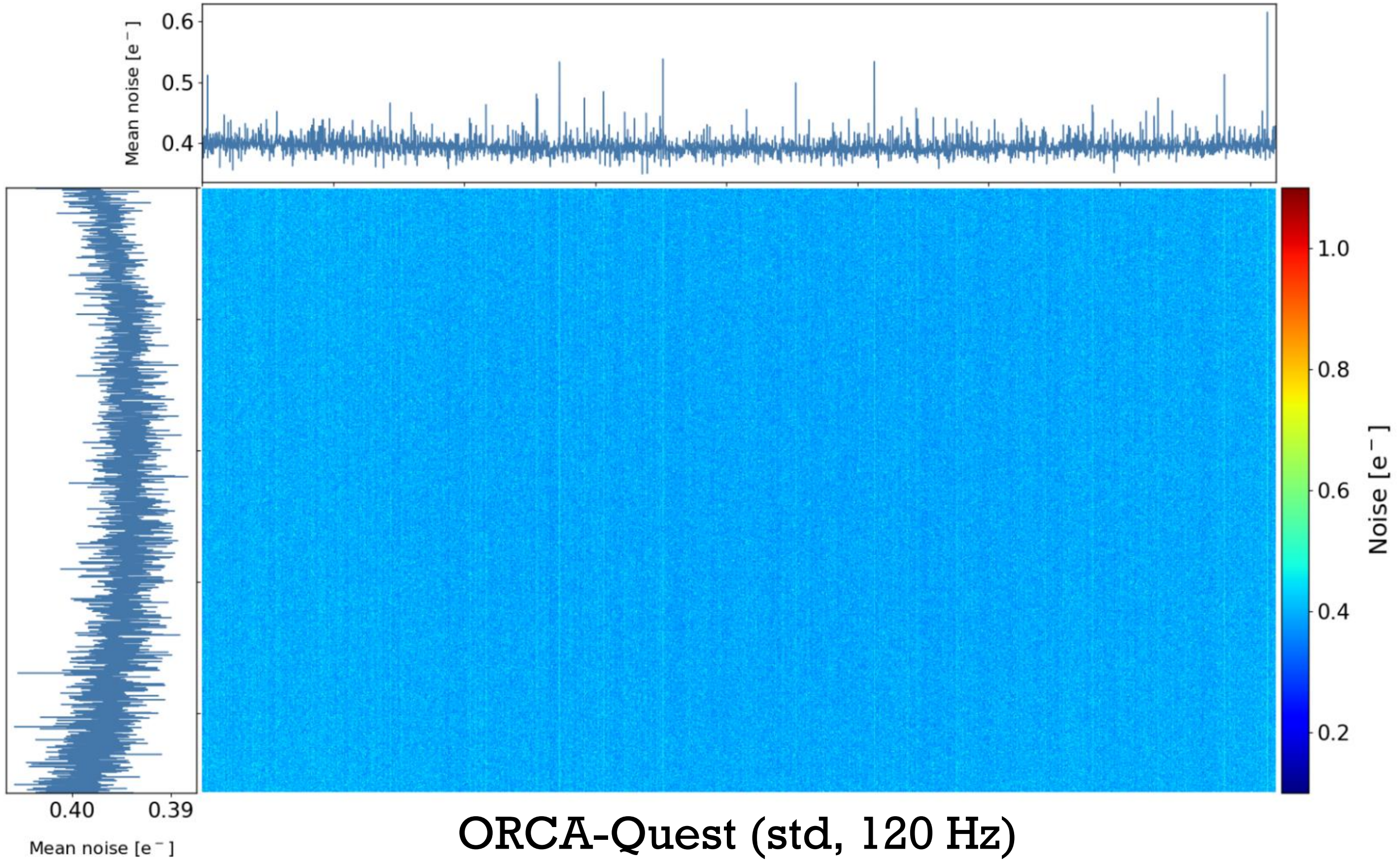

ORCA-Quest (std, 120 Hz)

timothy.marley15@imperial.ac.uk

Noise correlation comparison

- For uncorrelated noise, we expect noise to increase with $\sqrt{N}$ pixels binned.
- The deviation from this scaling is a measure of the noise correlation.
- The ORCA Quest looks much better than the ORCA Fusion in this regard.

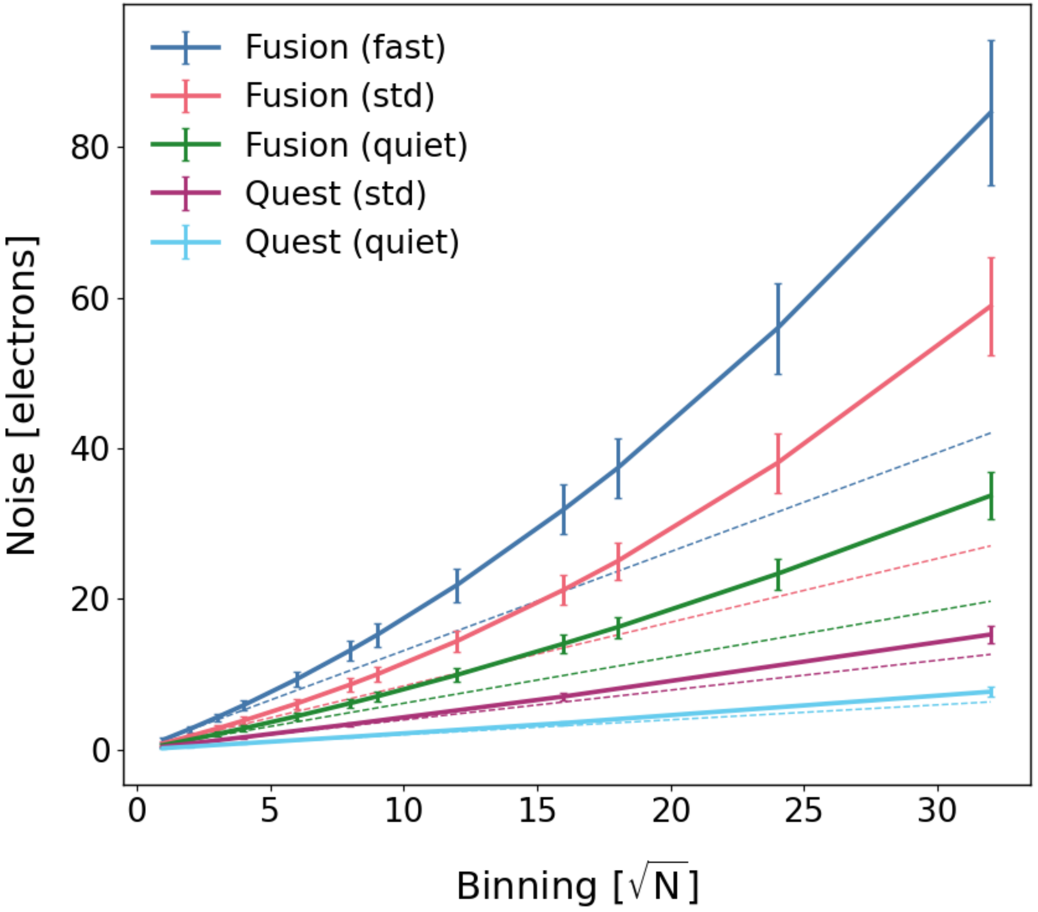

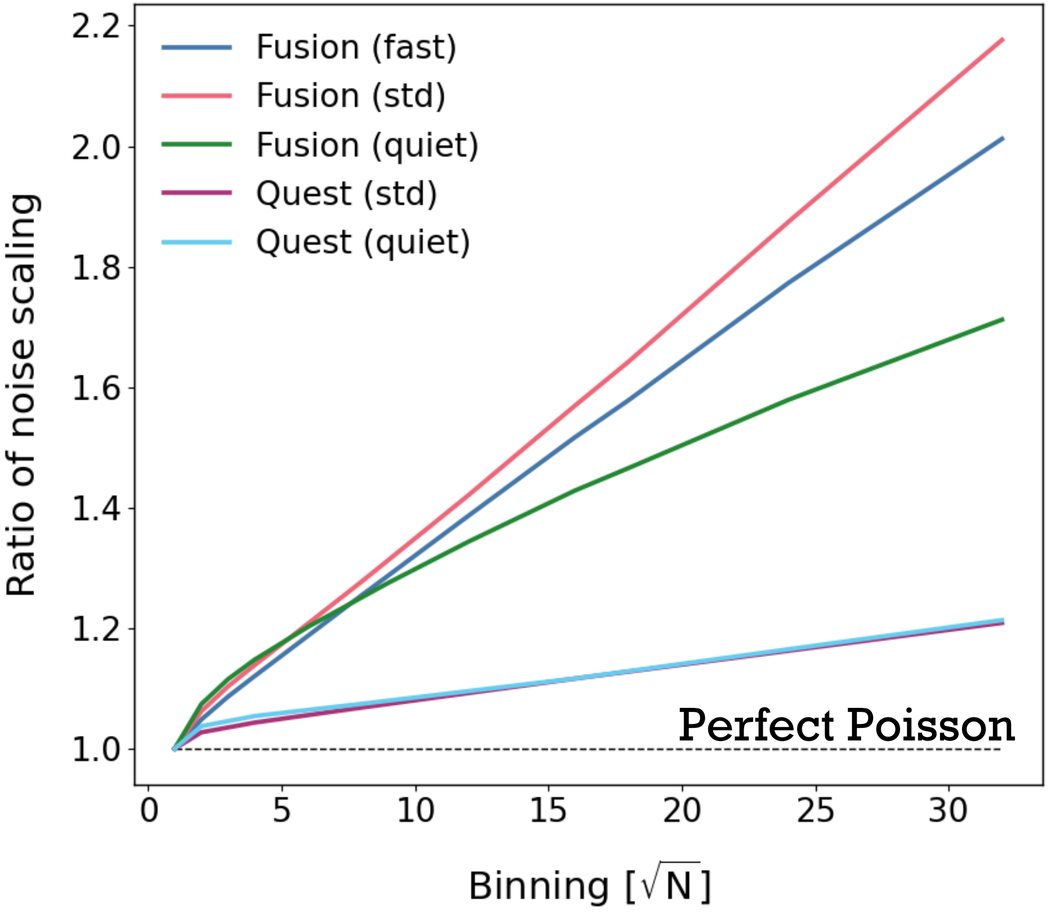

timothy.marley15@imperial.ac.uk

Alphas with ORCA Quest

- Testing operational stability with 37 Bq ^{252}Cf source in 50 Torr CF_4.
- The new camera produces very good-looking images!
- The optical distortion and lens field curvature are visible towards the edges of the image.

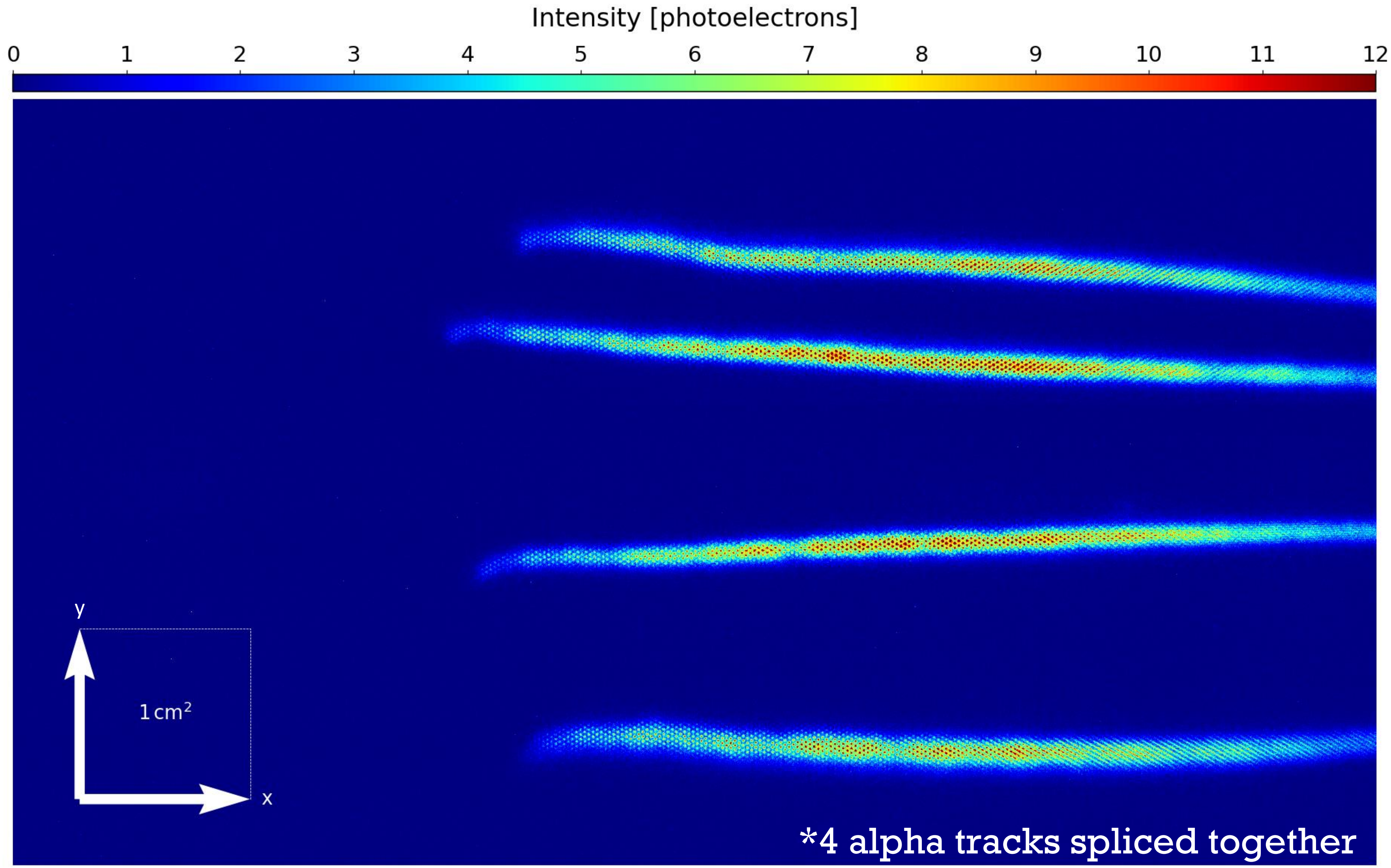

Afterglow with ORCA Quest

- In the following frame of each alpha track, we see an afterglow of ~1 photoelectron in many pixels.
- This does not seem to vary with exposure time.
- We are in contact with Hamamatsu.

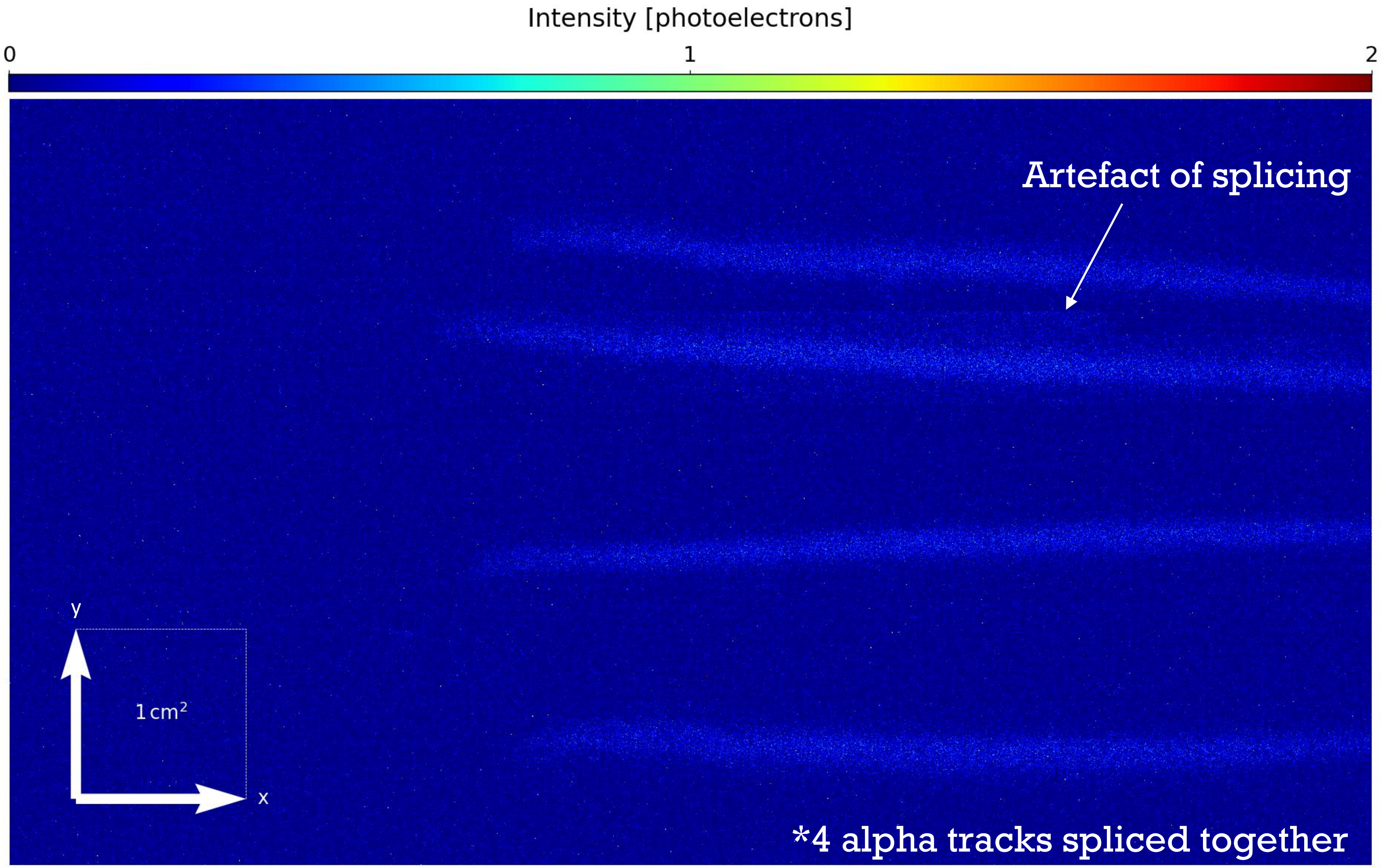

Alphas in the ITO strips

- The signals from alpha tracks create a ‘ripple’ in the ITO strips.
- ITO strips 1 & 62, 2 & 62 etc. are connected. This is ok for nuclear recoils as no tracks will be longer than 5 cm.

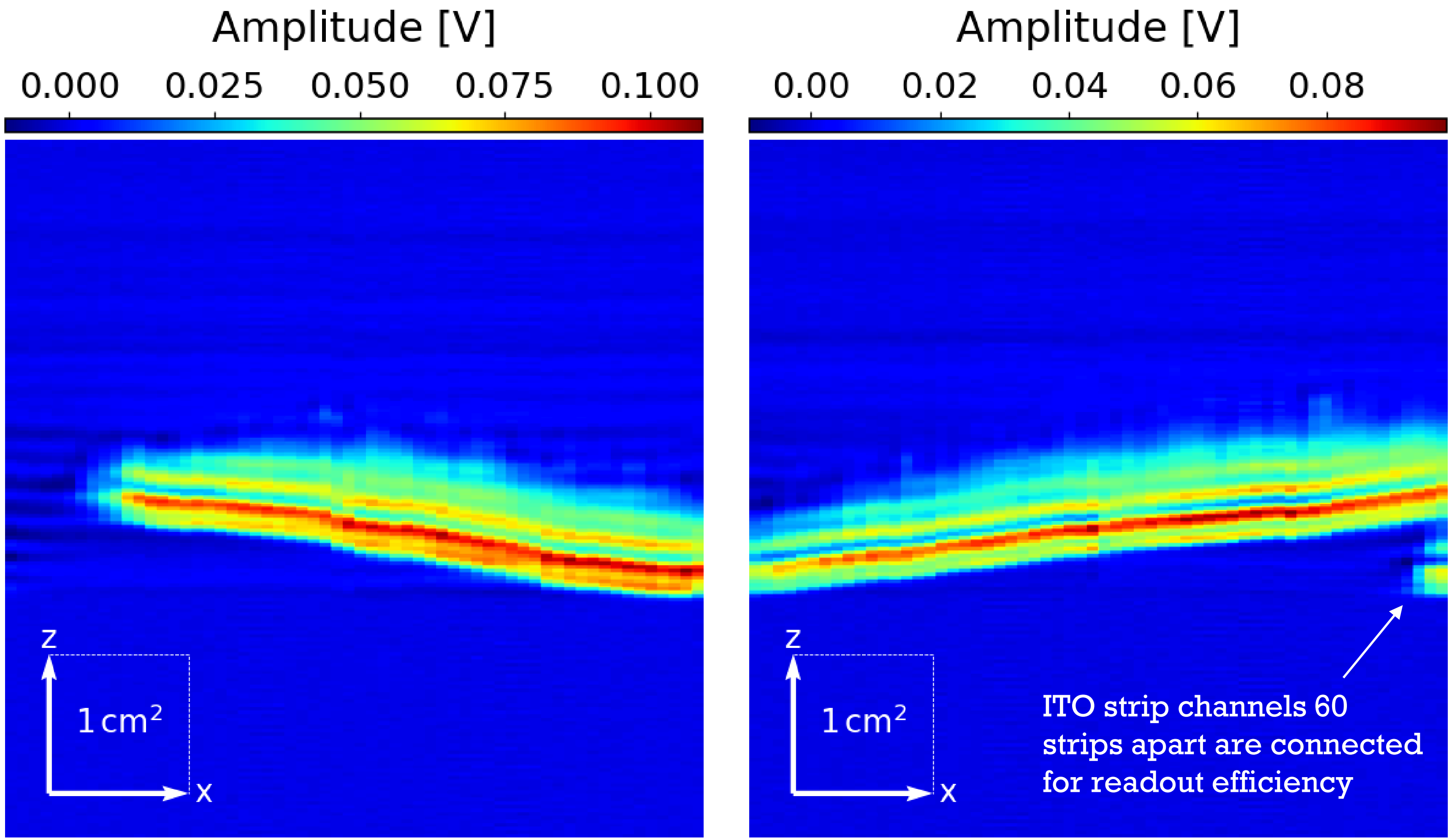

Sparks

- We see sparks occasionally from very high energy events.
- The electronics recover quickly after, but the recorded waveforms appear unsettling.
- Sometimes we see sparks on the pillar holes (described earlier).
- The spark rate is not currently concerning.

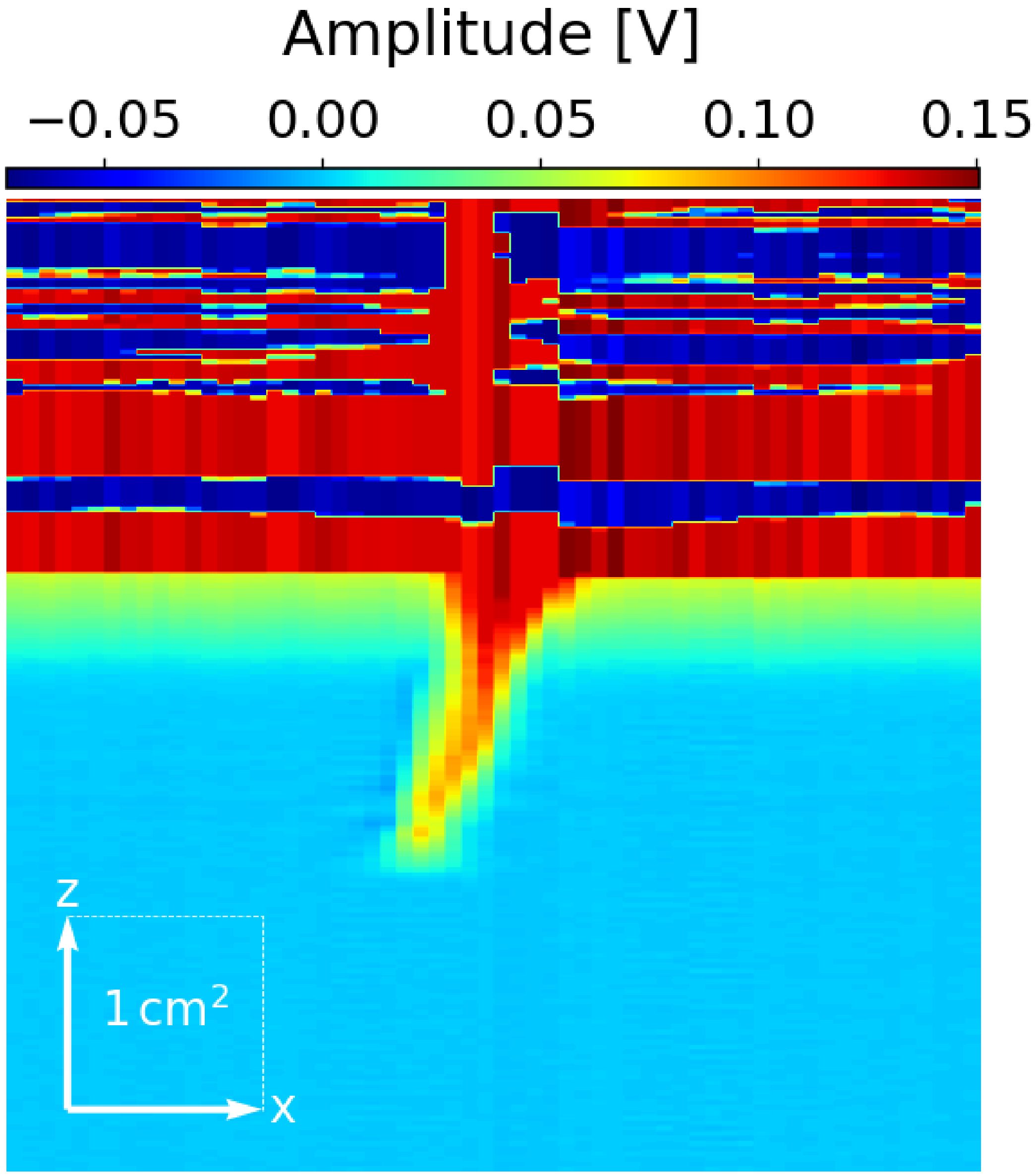

Calibration with ^{55}Fe

- The energy resolution at 'alpha-stable' voltages is a bit worse than the maximum achievable resolution.
- What limits the energy resolution?
  - We have not yet applied flat fielding to the ITO.
  - The camera needs better flat fielding.

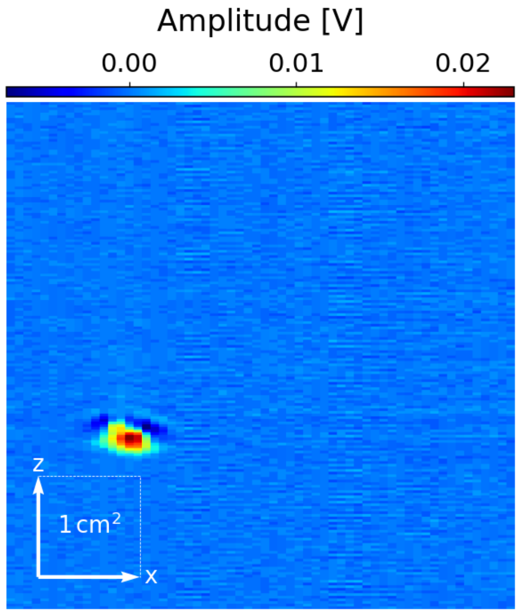

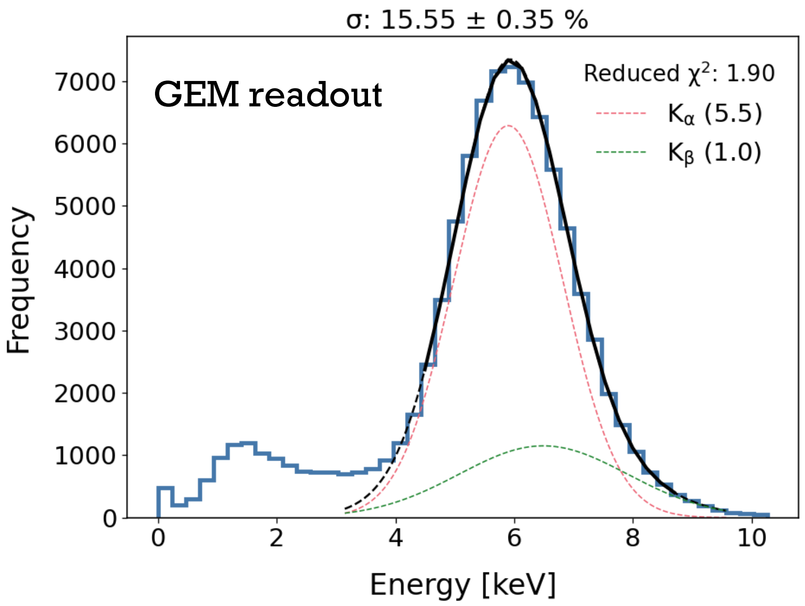

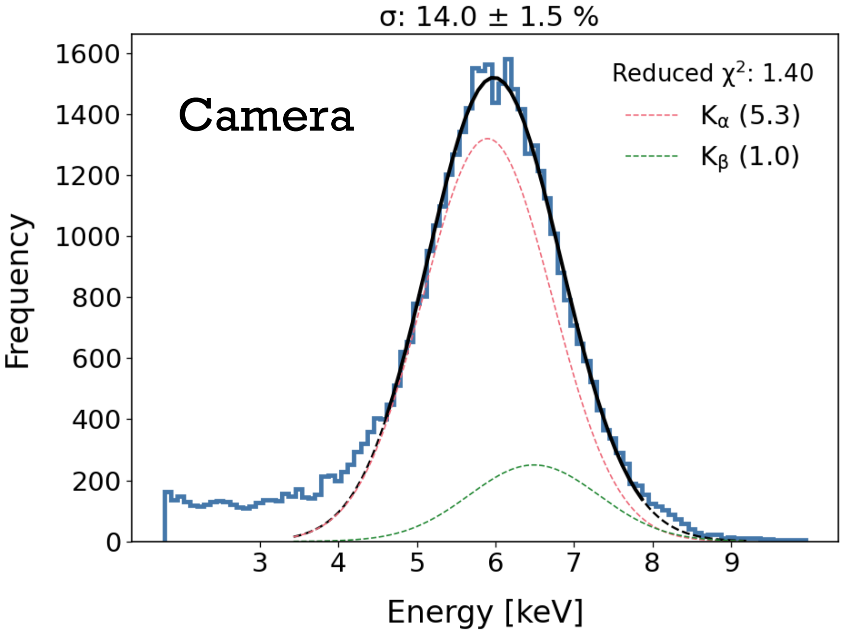

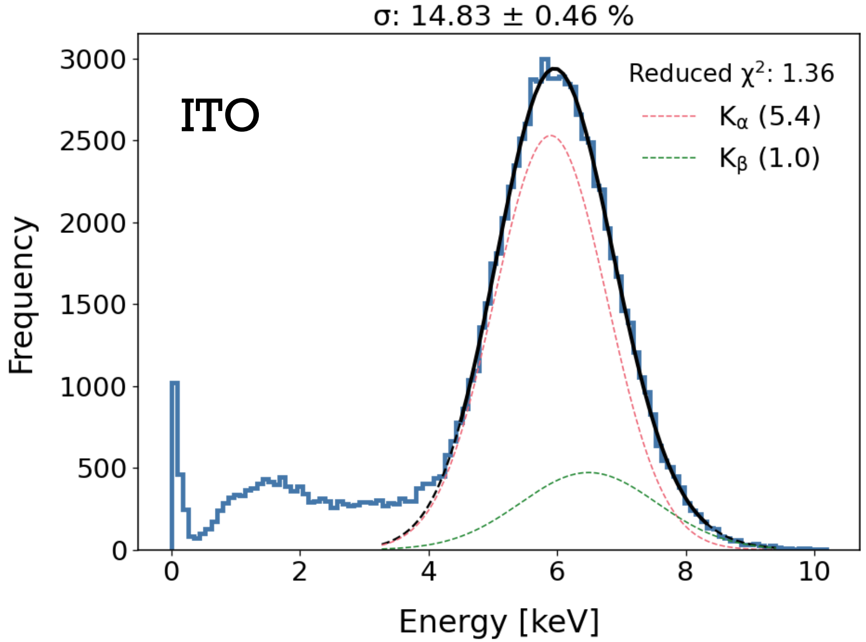

Loss of gain over time

- We are currently investigating the reason for a loss of gain over time.
- The decline was ~0.8%/hr.
- Is it due to outgassing?
- Is it due to damage?

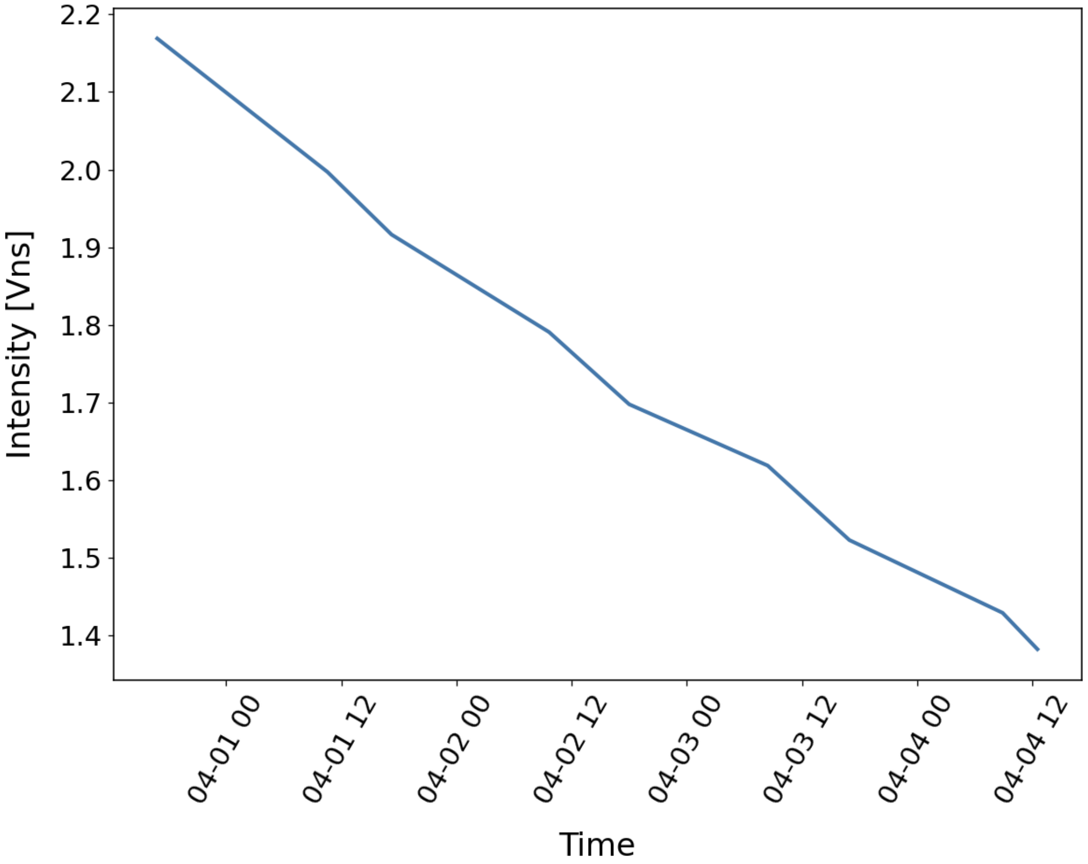

timothy.marley15@imperial.ac.uk

NILE facility

- NILE facility is at TS2, ISIS
- We packed up the chamber and moved it from lab 7 to NILE mid-May.

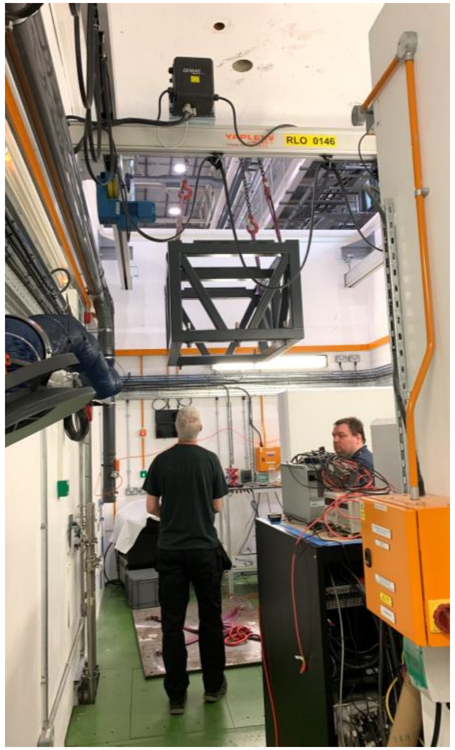

Table installed with lead under-shield

Chamber driven over to NILE

Assembling at NILE

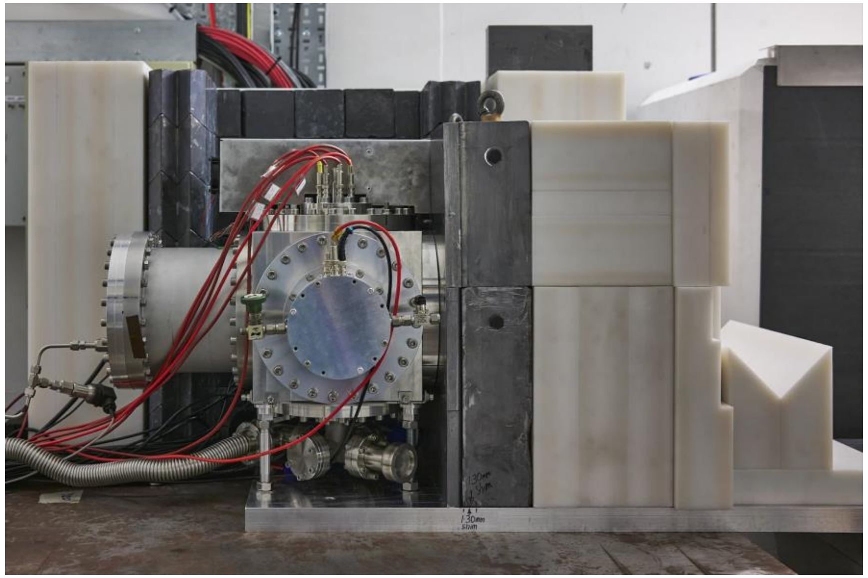

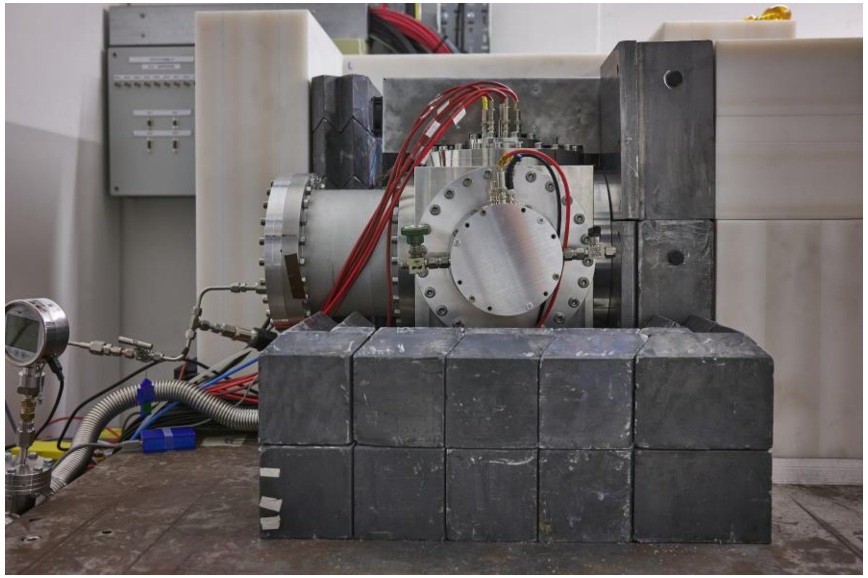

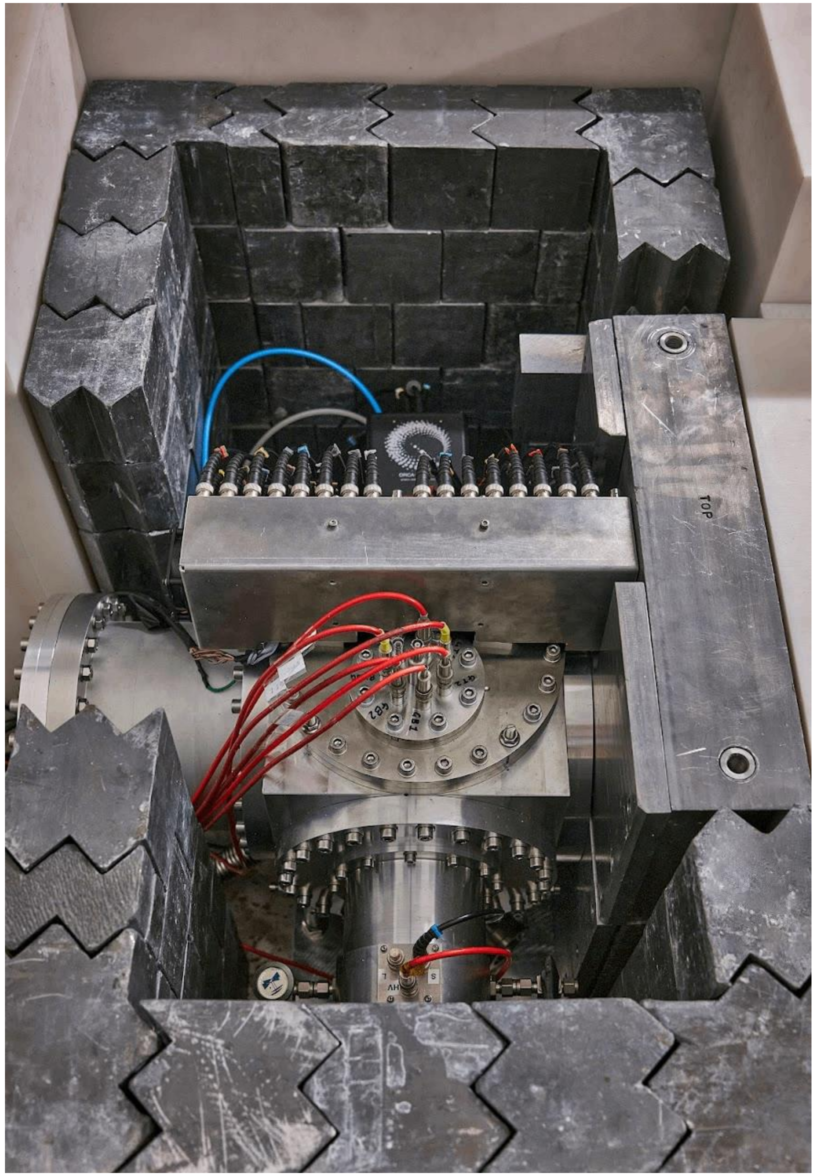

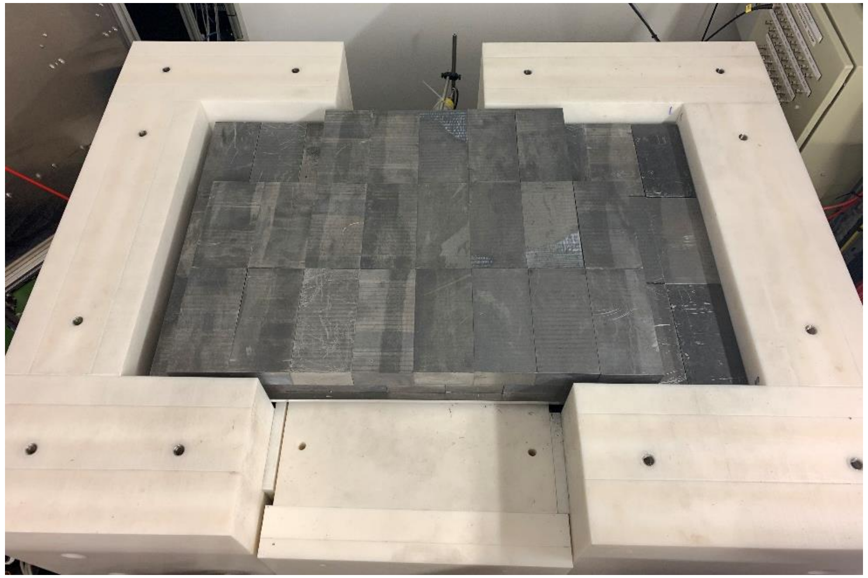

Exciting time!

Wish us luck!

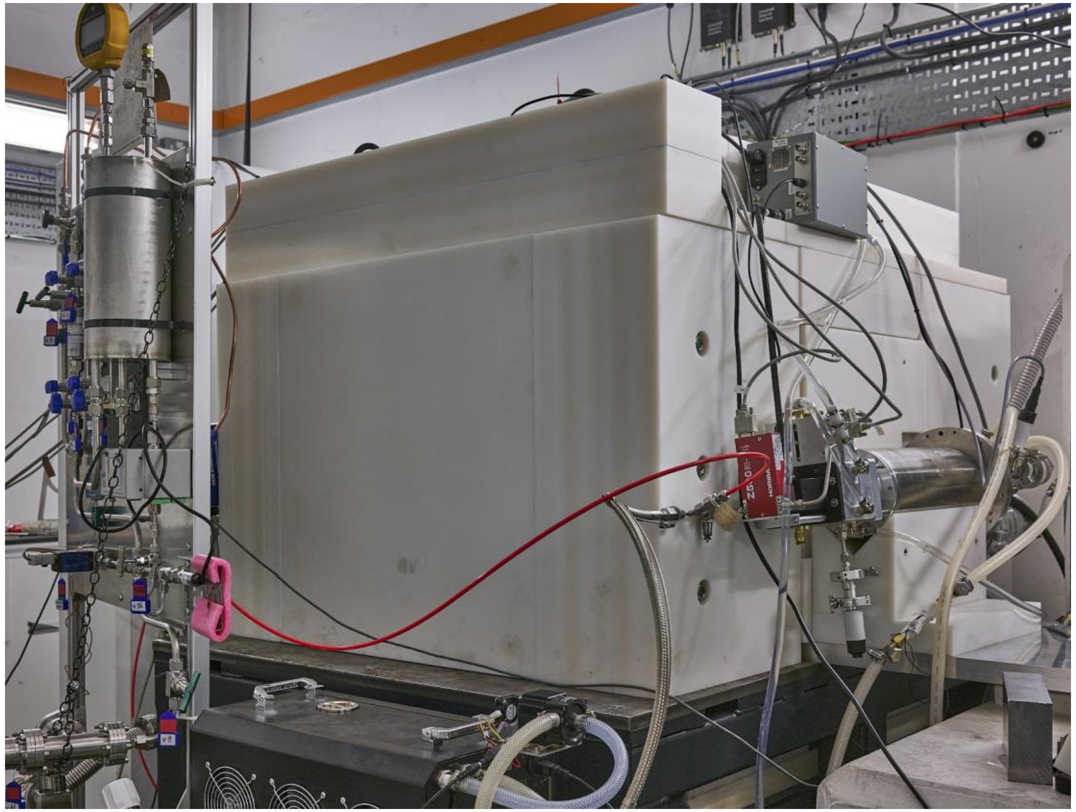

Summary

Experiment paper:
https://doi.org/10.1016/j.astropartphys.2023.102853

- The MIGDAL experiment aims to make a conclusive detection of the Migdal effect, followed by a systematic study: first in pure CF4, then in other gases and mixtures.
- We have tested the operational stability of the detector and are able to simultaneously measure 5 keV electrons and higher energy alphas.
- G-GEMs work well in low pressure but come with caveats.
- We are awaiting first results of the DD neutron generator with our detector!

Reserve slides

Papers

- [1] A. Migdal Ionizatsiya atomov pri yadernykh reaktsiyakh, ZhETF, 9, 1163-1165 (1939).
- [2] A. Migdal Ionizatsiya atomov pri α- i β-raspade, ZhETF, 11, 207-212 (1941) .
- [3] M.S. Rapaport, F. Asaro and I. Pearlman K-shell electron shake-off accompanying alpha decay, PRC 11, 1740-1745 (1975).
- [4] M.S. Rapaport, F. Asaro and I. Pearlman L- and M-shell electron shake-off accompanying alpha decay, PRC 11, 1746-1754 (1975).
- [5] C. Couratin et al. , First Measurement of Pure Electron Shakeoff in the β Decay of Trapped 6He+ Ions, PRL 108, 243201 (2012).
- [6] X. Fabian et al., Electron Shakeoff following the β + decay of Trapped 19Ne+ and 35Ar+ trapped ions, PRA, 97, 023402 (2018).

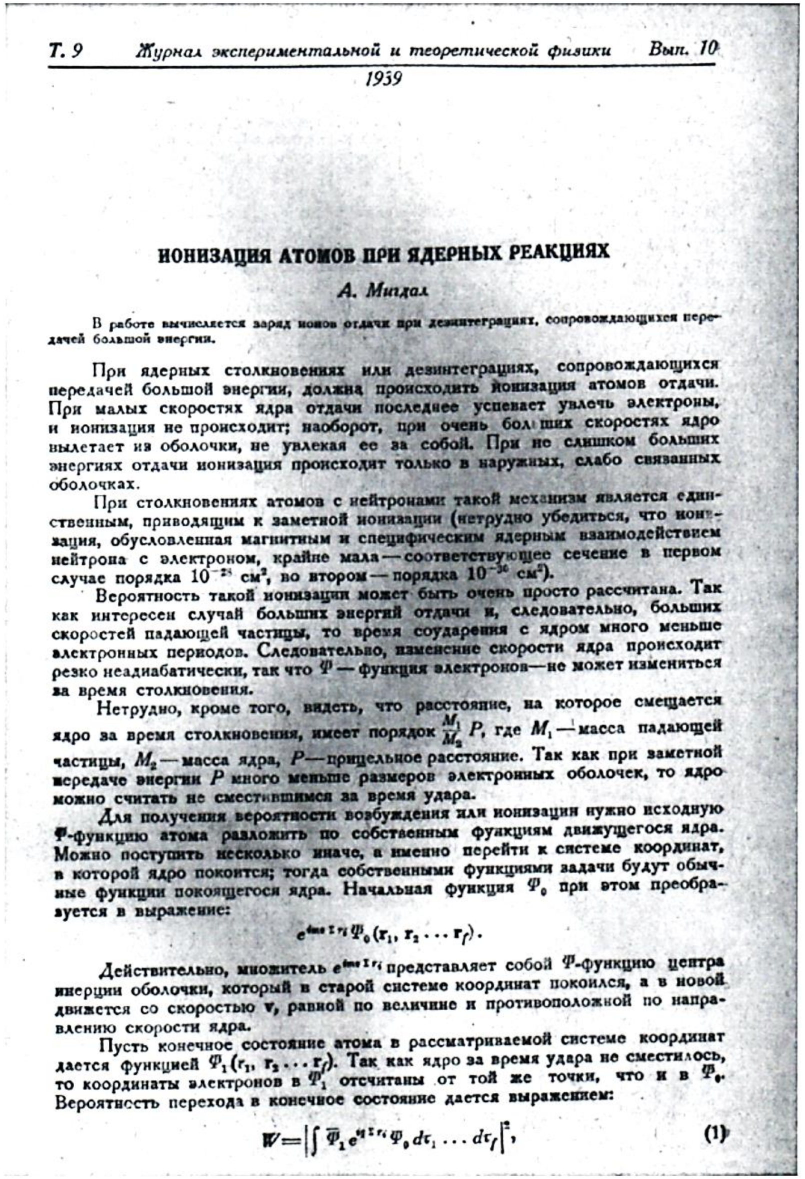

Т. 9 Журнал экспериментальной и теоретической физики Вып. 10

1939

ИОНИЗАЦИЯ АТОМОВ ПРИ ЯДЕРНЫХ РЕАКЦИЯХ

А. Мигдал

В работе вычисляется заряд ионов отдачи при дезинтеграциях, сопровождающихся передачей большой энергии.

При ядерных столкновениях или дезинтеграциях, сопровождающихся передачей большой энергии, должна происходить ионизация атомов отдачи. При малых скоростях ядра отдачи последнее успевает увлечь электроны, и ионизация не происходит; наоборот, при очень больших скоростях ядро вылетает из оболочки, не увлекая ее за собой. При не слишком больших энергиях отдачи ионизация происходит только в наружных, слабо связанных оболочках.

При столкновениях атомов с нейтронами такой механизм является единственным, приводящим к заметной ионизации (нетрудно убедиться, что ионизация, обусловленная магнитным и специфическим ядерным взаимодействием нейтрона с электроном, крайне мала — соответствующее сечение в первом случае порядка 10^{-25} см^2, во втором — порядка 10^{-30} см^2).

Вероятность такой ионизации может быть очень просто рассчитана. Так как интересен случай больших энергий отдачи и, следовательно, больших скоростей падающей частицы, то время соударения с ядром много меньше электронных периодов. Следовательно, изменение скорости ядра происходит резко неадиабатически, так что Ψ — функция электронов — не может измениться за время столкновения.

Нетрудно, кроме того, видеть, что расстояние, на которое смещается ядро за время столкновения, имеет порядок $\frac{M_1}{M_2}P$, где M_1 — масса падающей частицы, M_2 — масса ядра, P — прицельное расстояние. Так как при заметной передаче энергии P много меньше размеров электронных оболочек, то ядро можно считать не сместившимся за время удара.

Для получения вероятности возбуждения или ионизации нужно исходную Ψ-функцию атома разложить по собственным функциям движущегося ядра. Можно поступить несколько иначе, а именно перейти к системе координат, в которой ядро покоится; тогда собственными функциями задачи будут обычные функции покоящегося ядра. Начальная функция Ψ_0 при этом преобразуется в выражение:

$$e^{imv\Sigma r_i}\Psi_0(\mathbf{r}_1, \mathbf{r}_2 \dots \mathbf{r}_f).$$

Действительно, множитель $e^{imv\Sigma r_i}$ представляет собой Ψ-функцию центра инерции оболочки, который в старой системе координат покоился, а в новой движется со скоростью $\mathbf{v}$, равной по величине и противоположной по направлению скорости ядра.

Пусть конечное состояние атома в рассматриваемой системе координат дается функцией $\Psi_1(\mathbf{r}_1, \mathbf{r}_2 \dots \mathbf{r}_f)$. Так как ядро за время удара не сместилось, то координаты электронов в Ψ_1 отсчитаны от той же точки, что и в Ψ_0. Вероятность перехода в конечное состояние дается выражением:

$$W = \left| \int \overline{\Psi}_1 e^{iq\Sigma r_i} \Psi_0 \, d\tau_1 \dots d\tau_f \right|^2, \quad (1)$$

Signal / background

Component	Topology	D-D neutrons >0.5	D-D neutrons 5–15 keV	D-T neutrons >0.5	D-T neutrons 5–15 keV
Recoil-induced δ-rays	Delta electron from NR track origin	≈ 0	0	541,000	0
Particle-Induced X-ray Emission (PIXE)					
X-ray emission	Photoelectron near NR track origin	1.8	0	365	0
Auger electrons	Auger electron from NR track origin	19.6	0	42,000	0
Bremsstrahlung processes†					
Quasi-Free Electron Br. (QFEB)	Photoelectron near NR track origin	112	≈ 0	288	≈ 0
Secondary Electron Br. (SEB)	Photoelectron near NR track origin	115	≈ 0	279	≈ 0
Atomic Br. (AB)	Photoelectron near NR track origin	70	≈ 0	171	≈ 0
Nuclear Br. (NB)	Photoelectron near NR track origin	≈ 0	≈ 0	0.013	≈ 0
Photon interactions					
Neutron inelastic γ-rays (gas)	Compton electron near NR track origin	1.6	0.47	0.86	0.25
Random track coincidences	Photo-/Compton electron near NR track	≈ 0	≈ 0	≈ 0	≈ 0
Gas radioactivity					
Trace contaminants	Electron from decay near NR track origin	0.2	0.01	0.03	≈ 0
Neutron activation	Electron from decay near NR track origin	0	0	≈ 0	≈ 0
Secondary nuclear recoil fork	NR track fork near track origin	–	≈ 1	–	≈ 1
Total background	Sum of the above components		1.5		1.3
Migdal signal	Migdal electron from NR track origin		32.6		84.2

† These processes were (conservatively) evaluated at the endpoint of the nuclear recoil spectra.

ER and NR tracks in 50 Torr CF_4

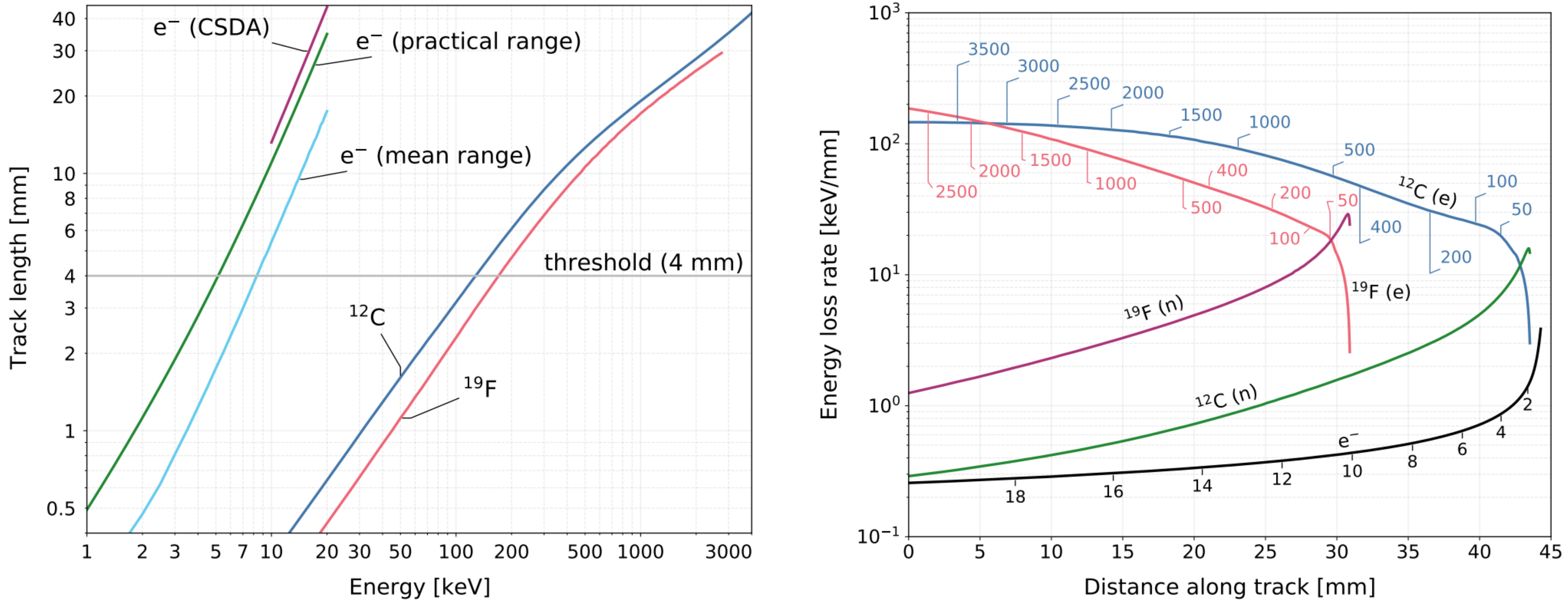

Figure 2: Left – Track length in CF_4 at 50 Torr for electrons (mean projected range calculated with Degrad [48], CSDA range with ESTAR [51], and the practical range formula from Ref. [52]), and mean projected range for carbon and fluorine ions from SRIM [49]). Right – Electronic and nuclear energy loss rates (CSDA) along carbon and fluorine ion tracks in CF_4 at 50 Torr, calculated with SRIM and electronic energy loss for 20 keV electrons obtained with ESTAR; called out values are interim particle energies (in keV) remaining at that point in the track.

timothy.marley15@imperial.ac.uk

Electron transport in 50 Torr CF_4

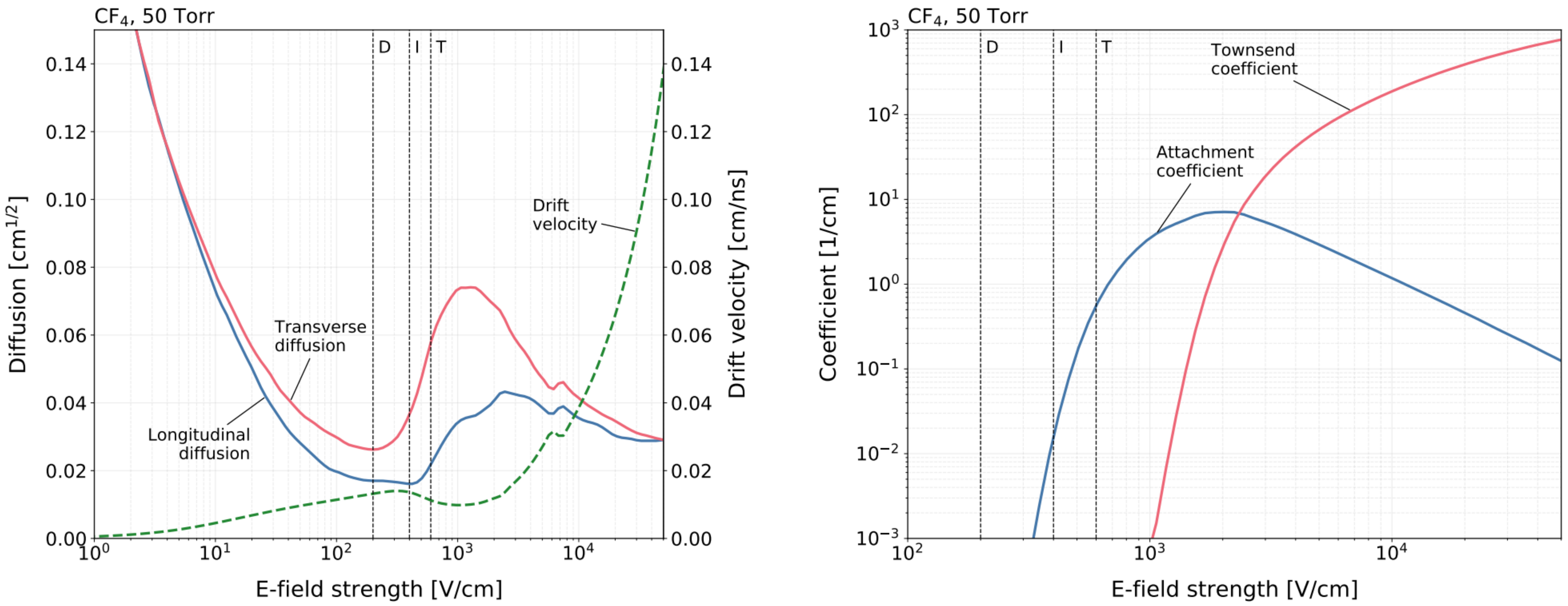

Figure 17: Electron transport properties of CF_4 at 50 Torr. Left – Drift velocity and diffusion. Right – Attachment and Townsend coefficients. Nominal fields in the drift (D), transfer (T) and induction (I) regions are indicated.

Migdal differential rates

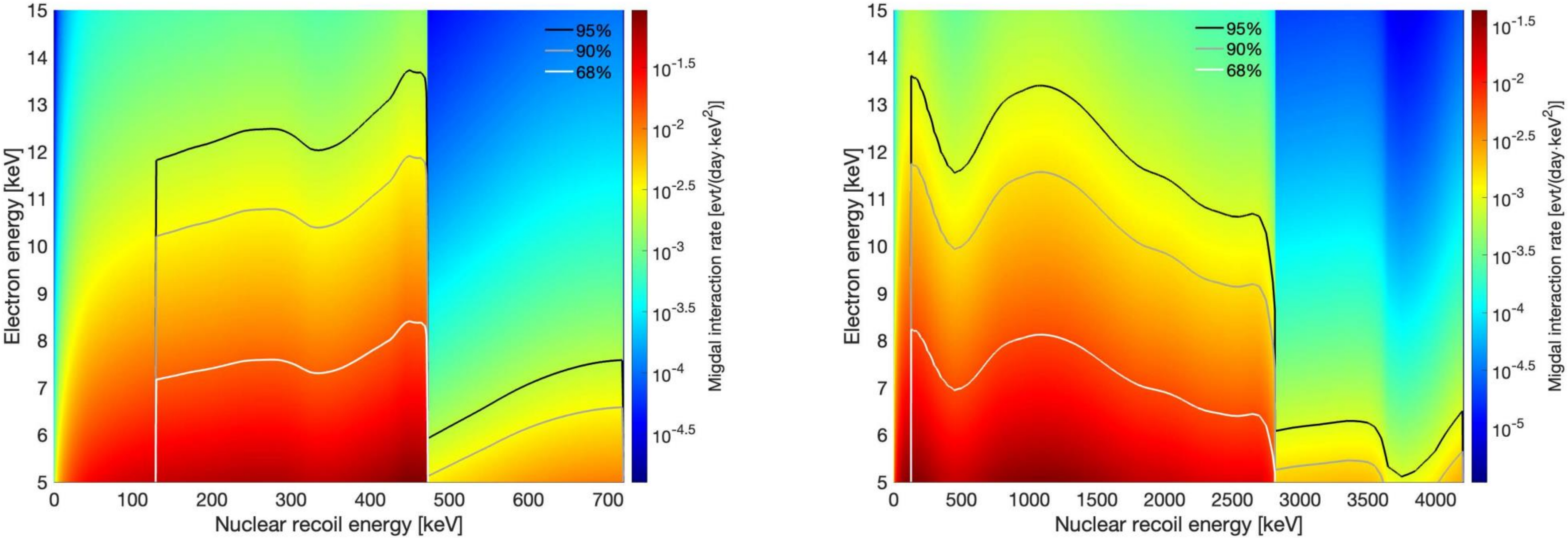

Figure 3: Double-differential Migdal rates for tracks contained in the OTPC from D-D (left) and D-T (right) generators. The contours are based on the NR thresholds of 130 keV and 170 keV for C and F, respectively. The area bound by the contours encompasses 68%, 90% and 95% of the signal.

Secondary nuclear recoils

Secondary recoils per million primary ions (TRIM) created within 1 mm from the vertex in 50 Torr CF_4, when the "visible" energy of the secondary is 5–15 keVee.

Primary ion	Secondary ion	
Fluorine	Fluorine	Carbon
500 keV	22,310	4,800
400	26,840	5,930
300	36,640	7,640
200	56,130	1,263
170	67,040	1,418
Carbon	Fluorine	Carbon
500 keV	6,250	1,210
400	7,950	1,610
300	11,380	2,310
200	17,310	3,700
130	26,120	5,770

~70,000 per million (worst case)

How many of these look like 5-10 keV electrons? Simulate several thousand more tracks using full chain, analyse image and recover track lengths (R_3) Can cut down to ~1 per 70,000 secondaries, retaining 87% electron detection efficiency (i.e. ~1 per million primary recoils).